Some aspects of β-$V_9Mo_6O_{40}$ reduction: TPR, XRD, SEM, IR and EPR spectroscopic studies

I. L. Botto,[a] M. Vassallo,[a] G. Fierro,*[b] D. Cordischi,[b] M. Inversi[b] and G. Minelli[b]

[a]*Centro de Quimica Inorganica (CEQUINOR), Facultad de Ciencias Exactas, Universidad Nacional de La Plata, CC 962, La Plata (1900), Argentina*

[b]*Centro di Studio del CNR su 'Struttura e Attività Catalitica di Sistemi di Ossidi' (SACSO) c/o Dipartimento di Chimica, Università 'La Sapienza', Piazza le A. Moro, 5, I-00185, Roma, Italy*

The β-$V_9Mo_6O_{40}$ phase, containing only 1/9 of the V atoms as V^{4+} ions, has been prepared by the solid-state reaction of suitable amounts of MoO_3 and V_2O_5 oxides heated to 923 K. The temperature-programmed reduction (TPR) analysis of the β-$V_9Mo_6O_{40}$ phase has been carried out up to 1273 K. The TPR profiles were always characterised by two peaks regardless of the experimental conditions. At the end of the first reduction peak, occurring at *ca.* 900 K, the β-$V_9Mo_6O_{40}$ phase disgregates by forming the MoO_2 and V_2O_3 oxides. The second reduction peak appears at higher temperature and corresponds to the reduction of MoO_2 to molybdenum metal. Both the as-prepared and reduced samples have been studied by X-ray powder diffraction (XRPD), IR and EPR spectroscopies as well as by scanning electron microscopy (SEM). The EPR analysis confirmed the presence of V^{4+} ions in the crystal lattice of the β-$V_9Mo_6O_{40}$ phase which is characterized by a metal–oxygen bonding different from those found for the pure MoO_3 and V_2O_5 oxides, as evidenced by the IR spectra. Prismatic crystals were observed by SEM for the as-prepared sample. The original morphology was essentially preserved upon H_2 reduction, but a widespread microroughness appeared at the surface of the prismatic crystals. At the beginning of the reduction process an increase of the V^{4+} species in the lattice was detected by EPR, giving rise to a gradual slight structural distortion. However, an oxidising treatment in air of the mildly reduced sample restores the original structure.

Introduction

Temperature programmed reduction (TPR) is a technique widely employed in catalysis to study the reducibility of oxide based systems. Most of the characterization work of a great number of transition-metal oxides has been carried out by TPR in relation to catalysts.[1] The pure MoO_3 and V_2O_5 oxides as well as some bimetallic compounds belonging to the V–Mo–O system have proved to be interesting and useful materials for industrial oxidation processes.[2–5] The reduction steps of the V_2O_5–MoO_3 containing binary compounds can be identified by well defined ranges of temperature. However, the extent of reduction of these materials depends on several factors, such as the experimental conditions and whether the oxides are bulk or supported.[6] The $Mo^{6+} \rightarrow Mo^{4+}$ reduction step occurs between 873 and 1073 K for bulk MoO_3, whereas the $Mo^{4+} \rightarrow Mo^0$ reduction is observed between 1113 and 1183 K.[6] These temperatures are about 100 K higher than those observed for Al_2O_3-supported material. On the other hand the TPR patterns of bulk V_2O_5 reported in literature show at low H_2 concentration some peaks between 900 and 1100 K which were associated to a stepwise $V_2O_5 \rightarrow V_2O_3$ reduction process occurring through the V_6O_{13}, VO_2, V_4O_7 intermediates.[1,7]

The influence of experimental parameters on the reduction temperature has been recently analysed. The TPR profile is characterized by one peak for a H_2 concentration equal to 35% whereas the splitting into more peaks as well as a considerable shift toward higher temperatures was observed at lower H_2 concentration.[8] However, in both cases V^{3+} was the stable final species.[6]

On the other hand, in mixed oxides the reactivity of each metallic element is reciprocally affected through a cooperative catalytic effect.[6,9] In this work the structural and reduction properties of the β-$V_9Mo_6O_{40}$ phase have been investigated. The β-$V_9Mo_6O_{40}$ oxide belongs to the V–Mo–O system and is now recognized to be a mixed-valence compound having 1/9 of the vanadium atoms as V^{4+} [10,11] while, on the contrary, in earlier studies it was erroneously formulated as $V^{5+}{}_2Mo^{6+}O_8$.[12] The $V_9Mo_6O_{40}$ phase is structurally related to V_2O_5 and, as recently reported, can be found in both orthorhombic (α) and monoclinic (β) forms.[10] Although there are not many data about the β phase, both structures seem to be closely related on the basis of their XRD patterns.[10]

Since the simultaneous presence of V^{4+}, V^{5+} and Mo^{6+} ions may affect the evolution of lattice oxygen and, consequently, the solid reducibility, the aim of this work is to study the thermal reduction of the β-$V_9Mo_6O_{40}$ phase in comparison with that of the MoO_3 and V_2O_5 pure oxides. In particular the effect of the V-reduced species on the reducibility of the remaining components has been investigated.

The study was performed by using quali- and quantitative temperature-programmed reduction (TPR), X-ray powder diffraction (XRPD), IR and EPR spectroscopies. Finally, the morphology and topical chemistry of the as-prepared and reduced material were also investigated by scanning electron microscopy (SEM) and by energy dispersive spectroscopy (EDS).

Experimental

Preparation

The β-$V_9Mo_6O_{40}$ phase was obtained by a solid-state reaction between suitable amounts of MoO_3 (prepared by decomposition of analytical grade ammonium heptamolybdate tetrahydrate) and V_2O_5 (prepared by decomposition of analytical grade ammonium vanadate) upon heating the mixture of pure oxides to 923 K. Intermediate milling from 573 to 923 K with steps of 50 K and a thermal treatment for 24 h at the final temperature completed the synthesis.

X-Ray powder diffraction

The XRD powder patterns of the as-prepared and reduced β-$V_9Mo_6O_{40}$ phase were obtained with a fully automated Philips

PW 1729 diffractometer equipped with an IBM PS2 computer for data acquisition and analysis. Scans were taken by using Cu-Kα (nickel-filtered) radiation.

Temperature-programmed reduction (TPR)

TPR measurements were performed both in Rome up to 1000 K and in La Plata up to 1273 K. In Rome the TPR runs, giving also the quantitave analysis of both the H_2 consumed and the H_2O formed upon reduction, were carried out in a previously described apparatus.[13] It consists of two parts: (1) a flow system to perform the TPR measurements by applying a stream of diluted hydrogen, and (2) a BET-type vacuum line where the sample pretreatment, trapping of the water released during the reduction and measurement of its quantity can be effected.[13] Ultrapure gases, H_2, N_2, O_2 and He (purity > 99.99%) were employed with no further purification. A four-channel electronic mass-flow controller (UCAR Instruments, Model MFB 30) was used for fixing accurately the flow rates of each gas. A temperature controller (Leeds & Northrup Instrument, Model Electromax V Plus) was used for the temperature programs. Nitrogen-diluted hydrogen crossed, at a fixed rate, the reference compartment, a hot wire (HW) detector from Carlo Erba (Model HWD 450), then the reactor containing the sample, and, finally, *via* a cold trap, the other compartment of the HW detector. The HW detector and the temperature controller were connected to an IBM computer and both the H_2 uptake and the heating rate were digitally acquired and processed. No interference on the TPR profiles caused by mass transfer limitations or dispersion effects was observed under our experimental conditions.[13,14] Samples used for the TPR measurements have the consistency of a fine powder. A quartz-glass reactor with a porous septum was used and the sample loading was *ca.* 0.035 g. The experimental operating variables (*i.e.* the initial H_2 concentration, $c_0 =$ 2.52 μmol ml^{-1}, the initial amount of reducible species, $S_0 =$ 270–340 μmol, and the total flow rate, $V = 40$ ml min^{-1}) were carefully chosen in order to obtain optimum reduction profiles.[13,14] Before starting a TPR run, each sample was pretreated *in situ* under flowing O_2 at 773 K for 0.5 h, flushed with N_2 for 0.33 h and, finally, cooled in N_2 at room temperature. A standard TPR run consisted of (i) an initial treatment in the reducing stream (40 ml min^{-1} of 6% v/v H_2 in N_2) at room temperature for 0.01 h; (ii) temperature programming; (iii) keeping the sample at the final temperature for 0.33 h and (iv) outgassing of the sample at the final temperature for 0.33 h. Three different heating rates, β, of 5, 2.5 and 1 K min^{-1}, were used. The total H_2 consumption was determined by: (*a*) transmitting the HW detector output to an amplification and integration system (Shimadzu Instruments, Model Chromatopac C-RIB) and (*b*) estimating the water released during the reduction through a stepwise expansion into a calibrated zone of the vacuum line. Peaks in the TPR profiles were characterized by the temperature corresponding to the maximum H_2 consumption rate, T_M. Qualitative TPR measurements were carried out in La Plata in a home-made TPR apparatus, from 293 to 1273 K, under experimental conditions (H_2 concentration, total flow rate, heating rate, sample loading) similar to those employed in Rome for the quantitative measurements. The H_2 consumption rate was monitored by a thermal conductivity cell. The data from Rome and La Plata for the same range of temperature confirmed each other.

IR spectroscopy

The IR spectra were recorded in the wavenumber range 1200–300 cm^{-1} by using a Perkin Elmer 580-B spectrophotometer and KBr pellets.

EPR spectroscopy

The EPR measurements were determined at X-band either at room temperature and at 77 K. A Varian E-9 spectrometer, equipped with an on-line computer for data treatment, was used. The absolute concentration of the paramagnetic species was calculated from the integrated area of the spectra. Pure vanadyl compounds as crystalline powders, *i.e.* vanadyl acetylacetonate, $VO(acac)_2$, vanadyl sulfate, $VOSO_4 \cdot 5H_2O$ and vanadyl tetraphenylporphyrinate, VO(TPP), were used as calibration standards. In order to fill up the resonant cavity, a suitable amount of standards or of the $V_9Mo_6O_{40}$ sample was placed in a capillary and then inserted into the EPR silica tube, thus obtaining the so-called 'infinite geometry'. All the instrumental parameters, except the gain, were fixed and kept constant. Under these conditions the number of spins cm^{-1}, N, of two samples a and b, are related by the following equation:

$$N_a = N_b \frac{g_b S_b (S_b + 1) A_a}{g_a S_a (S_a + 1) A_b} \quad (1)$$

where A are the integrated areas (measured at the same temperature), g and S the average g (g_{av}) and the spin values, respectively. The g values were referenced to the sharp peak of the E'_1 centre at $g = 2.0008$ formed by UV irradiation of the silica Dewar used as sample holder.[15] Two standards, *i.e.* $VOSO_4 \cdot 5H_2O$ and $VO(acac)_2$, gave a single exchange-narrowed line at RT and 77 K, whereas the EPR spectrum of VO(TPP) was characterised by a resolved hyperfine structure. In all cases the Curie law was obeyed with the ratio of the integrated areas at 77 K and RT in the range 3.5–3.8. With this respect it may be useful to recall that, if the Curie law is followed, the ratio of the integrated areas measured at two different temperatures is simply equal to the ratio of the reciprocal temperatures (273/77 = 3.86). For the standards, which are pure compounds, the number of spins cm^{-1}, N, was calculated according to the formula $N = 6.02 \times 10^{23}\, d/M$, where d is the linear density (g cm^{-1}) of the solid in the capillary and M is the molecular mass. The ratio N/A measured at RT as well as at 77 K was almost constant (10% maximum deviation) for all the standards and was consistent with eqn. (1). The spins cm^{-1} of the β-$V_9Mo_6O_{40}$ sample was obtained by employing the average of the N/A values found for the three standards and, finally, the spins g^{-1} was calculated by dividing the spins cm^{-1} by the linear density, d (g cm^{-1}) of the solid.

Scanning electron microscopy (SEM)

A Philips 505 scanning electron microscope equipped with an EDAX 9100 energy dispersive detector was used to study the morphology of both the as prepared and reduced samples and to make topical chemical analysis.

Results

X-Ray powder diffraction

Fig. 1A(*a*), (*b*) shows the XRPD patterns of the as prepared sample and of the reference β-$V_9Mo_6O_{40}$ phase[10] respectively. The diffraction patterns appear to be very similar and no extra lines, except those of the reference compound, were found for the as-prepared specimen.

Fig. 1B(*a*)–(*c*) shows the XRPD patterns of the reduced sample as recovered after different TPR runs (*vide infra*). For the sake of comparison, in Fig. 1B the XRPD data for MoO_2 (ASTM 32 671), V_2O_3 (ASTM 34 107) and Mo (ASTM 42 1120) are also shown. The peak intensity for the reduced samples decreases from the diffraction pattern (*a*) to the diffraction pattern (*c*) suggesting that a different crystallinity was attained depending on the final temperature of the TPR runs.

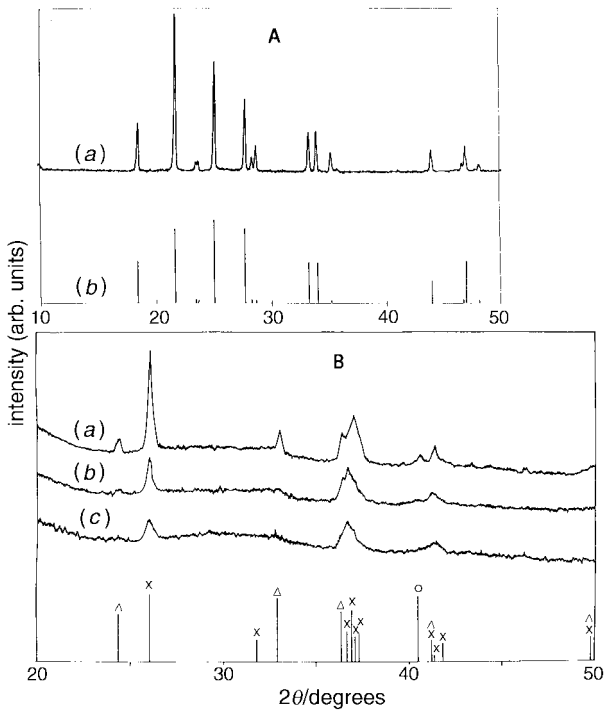

Fig. 1 A, XRPD analysis: (*a*) as-prepared sample; (*b*) reference spectrum taken from literature (see ref. 10). B, Comparative XRPD patterns of β-$V_9Mo_6O_{40}$ samples recovered after the first reduction peak in the TPR runs at different heating rates, β: (*a*) $\beta = 5$ K min^{-1}, (*b*) $\beta = 2.5$ K min^{-1}, (*c*) $\beta = 1$ K min^{-1}. Reference spectra taken from the ASTM X-Ray Powder Data File: (×) MoO_2 (ASTM 32-671); (△) V_2O_3 (ASTM 34-107); (○) Mo (ASTM 42-1120).

Temperature-programmed reduction

Fig. 2 shows the TPR profile at $\beta = 2.5$ K min^{-1} of the β-$V_9Mo_6O_{40}$ sample. The reduction profile is characterised by two peaks whose maxima are located at $T_M = 863$ and 1103 K. Also the TPR profile recorded at a heating rate of 5 K min^{-1} is characterised by two peaks which, with respect to those found at 2.5 K min^{-1}, are slightly shifted towards higher temperatures (T_M values at *ca.* 900 and 1130 K). Table 1 lists quantitative results and T_M values for the first reduction peak which appears in the TPR runs at different heating rates. The increase of the T_M values on increasing the heating rate is expected on the basis of non-isothermal reduction theory.[14] Under similar experimental conditions the TPR profile of pure MoO_3 revealed the formation of MoO_2 at a temperature close to 1000 K followed by the reduction of MoO_2 to Mo^0 at higher temperature (*ca.* 1120 K). For pure V_2O_5 a peak was observed at *ca.* 1000 K corresponding to reduction to V_2O_3.

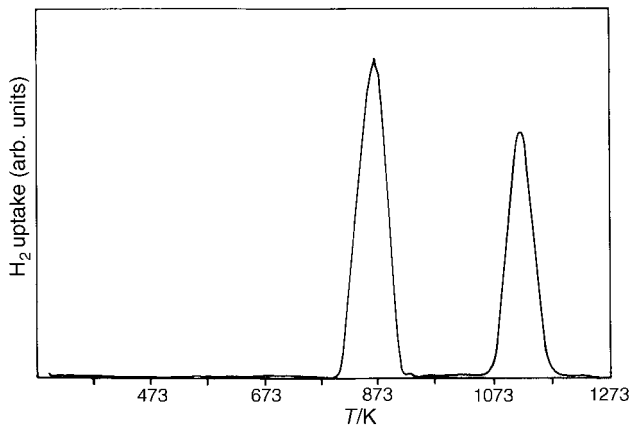

Fig. 2 TPR of β-$V_9Mo_6O_{40}$ ($\beta = 2.5$ K min^{-1})

Table 1 Quantitative TPR results and T_M values for the first reduction stage of the β-$V_9Mo_6O_{40}$ phase

T_M/K	β/K min^{-1}	loading/g	$(S_0)_{exp}$/μmol	$(S_0)_{theor.}$[a]/μmol
918	5	0.03246	365	281
863	2.5	0.03403	275	295
833	1.0	0.03711	321	321

[a]The theoretical S_0 values have been calculated on the basis of the following stoichiometry:

$$V_9Mo_6O_{40} + 29/2\ H_2 \rightarrow 9/2\ V_2O_3 + 6\ MoO_2 + 29/2\ H_2O$$

and therefore represent both the amount of the H_2 consumed and the H_2O formed by reduction (see text).

These results are in agreement with those reported in literature.[1,4,16,17]

IR spectroscopy

Fig. 3A shows the IR spectrum of the as-prepared β-$V_9Mo_6O_{40}$ sample together with the IR spectra of V_2O_5 and MoO_3. Fig. 3B shows the IR spectra of the β-$V_9Mo_6O_{40}$ samples after different degrees of reduction and after re-oxidising treatments. In particular, in the latter figure, the spectrum 3B(*a*), taken as reference, corresponds to the original β-$V_9Mo_6O_{40}$ phase which, upon reduction in TPR runs stopped at 623, 723 and 823 K gave, respectively, spectra 3B(*b*)–(*d*). Spectra 3B(*e*), (*f*) were recorded after a re-oxidising treatment in air at 773 K for 1 and 24 h, respectively, of the sample reduced in the TPR run stopped at 823 K. The IR analysis was also made on the original β-$V_9Mo_6O_{40}$ phase reduced at temperatures >823 K: Fig. 3B(*g*), (*h*) show the spectra of samples recovered after TPR runs stopped at 923 and 1273 K, respectively. Finally in Fig. 3B(*i*) the spectrum of V_2O_3 formed by TPR of V_2O_5 stopped at 1273 K is shown.

EPR spectroscopy

Fig. 4 shows EPR spectra of the β-$V_9Mo_6O_{40}$ sample as prepared and after reduction in TPR runs stopped at 823 and

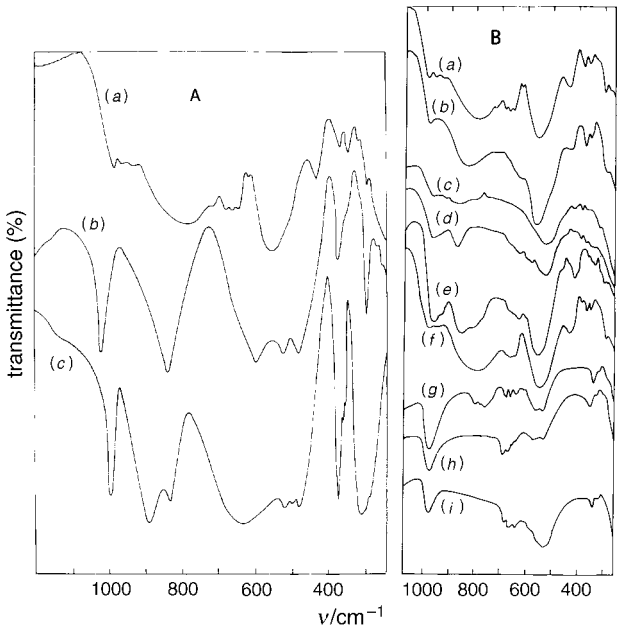

Fig. 3 A, IR spectrum of: (*a*) β-$V_9Mo_6O_{40}$, (*b*) V_2O_5, (*c*) MoO_3. B, Comparative IR spectra of: (*a*) original sample, (*b*) sample recovered after TPR at 623 K, (*c*) sample recovered after TPR stopped at 723 K, (*d*) sample recovered after TPR stopped at 823 K, (*e*) sample (*d*) reoxidised in air at 773 K for 1 h, (*f*) sample (*d*) reoxidised in air at 773 K for 24 h, (*g*) sample recovered after TPR stopped at 923 K, (*h*) sample recovered after TPR stopped at 1273 K, (*i*) V_2O_3 formed by TPR of V_2O_5 stopped at 1273 K.

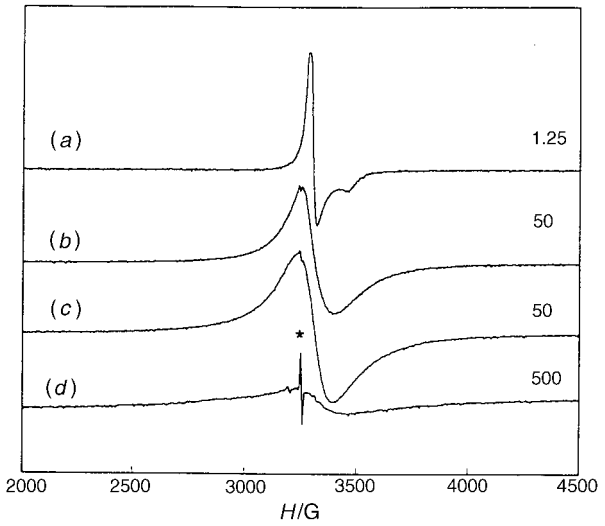

Fig. 4 EPR spectra of the β-$V_9Mo_6O_{40}$ phase: (*a*) as-prepared, recorded at 77 K; (*b*) as prepared, recorded at RT; (*c*) after TPR stopped at 823 K (recorded at RT); (*d*) after TPR stopped at 950 K (recorded at RT). The numbers on the spectra indicate the relative gain; the sharp peak labelled with * in spectrum (*d*) is from the photoinduced E1′ center at $g=2.0008$ formed by UV irradiation of the silica Dewar used as a sample holder.

950 K, respectively and Table 2 lists the results of the quantitative EPR analysis. It should be recalled that at 823 K the reduction process is just commencing whereas at 950 K the original β-$V_9Mo_6O_{40}$ phase was reduced to MoO_2 and V_2O_3.

SEM/EDS

Fig. 5 shows SEM micrographs of as-prepared and reduced β-$V_9Mo_6O_{40}$ samples. Energy dispersive spectroscopy (EDS) analysis was conducted on reduced samples (i) as recovered after the first reduction peak in the TPR runs at $\beta=5$, 2.5 and 1 K min^{-1} and (ii) as recovered after the second reduction peak in the TPR run at $\beta=2.5$ K min^{-1} (Fig. 2). Table 3 lists the results obtained from the EDS analysis. In Fig. 5(*d*) the arrow indicates the point where the spot analysis gave the highest content of vanadium. The morphology of the β-$V_9Mo_6O_{40}$ sample is essentially characterized by prismatic crystals in the oxidised state. Upon reduction the original morphology is still preserved but a widespread microroughness appears on the surface of most prismatic crystals.

Discussion

X-Ray powder diffraction

Fig. 1A shows that the diffraction pattern (*a*) of the as prepared sample matches almost perfectly the reference diffraction pattern (*b*) of the β-$V_9Mo_6O_{40}$ phase. It has been reported that Mo^{6+} can replace V^{5+} in the V_2O_5 structure giving a $(Mo_xV_{1-x})_2O_5$ solid solution with $0.1<x<0.28$.[12] In order to balance the excess of lattice charge caused by the replacement of V^{5+} by Mo^{6+}, the formation of paramagnetic V^{4+} species occurs. Moreover, on increasing x, a phase transformation is promoted and the V_2O_5 structure changes from orthorhombic to monoclinic when x is close to 0.2.[10] However, both structures remain structurally related being built up by edge-shared octahedra forming zigzag chains. Adjacent chains are connected to each other by corner-sharing octahedra. One of the most relevant difference between the orthorhombic and monoclinic structures is the displacement of the metal ions from the center of the octahedra. In the V_2O_5 structure, which can be regarded as ReO_3-type slabs connected by edge sharing,[12] all the metal ions of each ReO_3 slab are displaced in the same direction giving rise to a square-pyramidal coordination around vanadium ions characterized by a shortest V—O distance (1.58 Å).[18] In the monoclinic solid solution the metal atoms are shifted in opposite directions and their coordination tends to be octahedral. The $V_9Mo_6O_{40}$ phase, which is the active component of the coating V–Mo–O catalyst, appears as the Mo content is further increased. Two crystalline forms are known by this composition: the α phase, which is isostructural with V_2O_5, and the β phase, which is a member of the M_nO_{3n-1} homologous series with $n=3$ (it should be noted that V_2O_5 is the member with $n=2$).[19] When Mo^{6+} ions enter the V_2O_5 lattice, a modification not only of the geometry but also of the arrangement of the metal polyhedra occurs which can be described in terms of a CS shear structure.[20] As a result of this process, there is a decrease of the multiple bond character of the originally shortest V—O bond.

XRPD analysis of the reduced samples revealed that the main reduction products are MoO_2 and V_2O_3 at the final temperature of the first TPR peak. The diffraction line at 2θ *ca.* 40° belongs to Mo metal and appears in the diffraction pattern 1B(*a*) as a weak peak which then gradually disappears in the diffraction patterns 1B(*b*) and (*c*). The formation of a small amount of molybdenum metal, which is indeed quantitatively formed in the second TPR peak, is likely owing to a partial overlap of the two reduction steps occurring as the heating rate of the TPR run is increased (*vide infra*). The

Table 2 Results of the EPR analysis on oxidised and reduced β-$V_9Mo_6O_{40}$ samples

sample	linear density (*d*)/ g cm^{-1}	spin g^{-1} (N^0/M)[a]	spin cm^{-1} ($N=N^0d$/M)	g_{av}	A_{RT}[b]	A_{LN}[c]	A_{LN}/A_{RT}	$N/A_{RT}/10^{15}$	spin g^{-1}
$VOSO_4\cdot5H_2O$[d]	0.0084	2.37×10^{21}	1.99×10^{19}	1.99	4659	18270	3.9	4.27	
$VO(acac)_2$[d]	0.0050	2.26×10^{21}	1.13×10^{19}	2.0	2846	10820	3.8	3.97	
VO(TPP)[d]	0.0027	8.86×10^{20}	2.39×10^{18}	1.96	506	1902	3.8	4.72	
$V_9Mo_6O_{40}$ (fully oxidised)[e]	0.040			1.94	2282	6410	2.8		2.5×10^{20}
$V_9Mo_6O_{40}$ (fully oxidised)[f]	0.015			1.94	1139				3.3×10^{20}
$V_9Mo_6O_{40}$ (TPR at 823 K)[g]	0.013			1.94	1893	7383	3.9		6.3×10^{20}
$V_9Mo_6O_{40}$ (TPR at 950 K)[h]	0.013			1.94	70				0.2×10^{20}

[a]In the formula, N^0 and M are, respectively, Avogadro's number and the molecular mass. [b]Integrated areas, as measured at room temperature. [c]Integrated areas, as measured at liquid-nitrogen temperature. [d]Standards used for instrument calibration (see text). [e]As prepared (fully oxidised) $V_9Mo_6O_{40}$ phase loaded in an EPR tube. [f]As prepared (fully oxidised) $V_9Mo_6O_{40}$ phase loaded in a capillary. [g]Reduced $V_9Mo_6O_{40}$ sample, as recovered after the TPR run purposely stopped at 823 K (see text) and loaded in a capillary. [h]Reduced $V_9Mo_6O_{40}$ sample, as recovered after the TPR run purposely stopped at 950 K (see text) and loaded in a capillary.

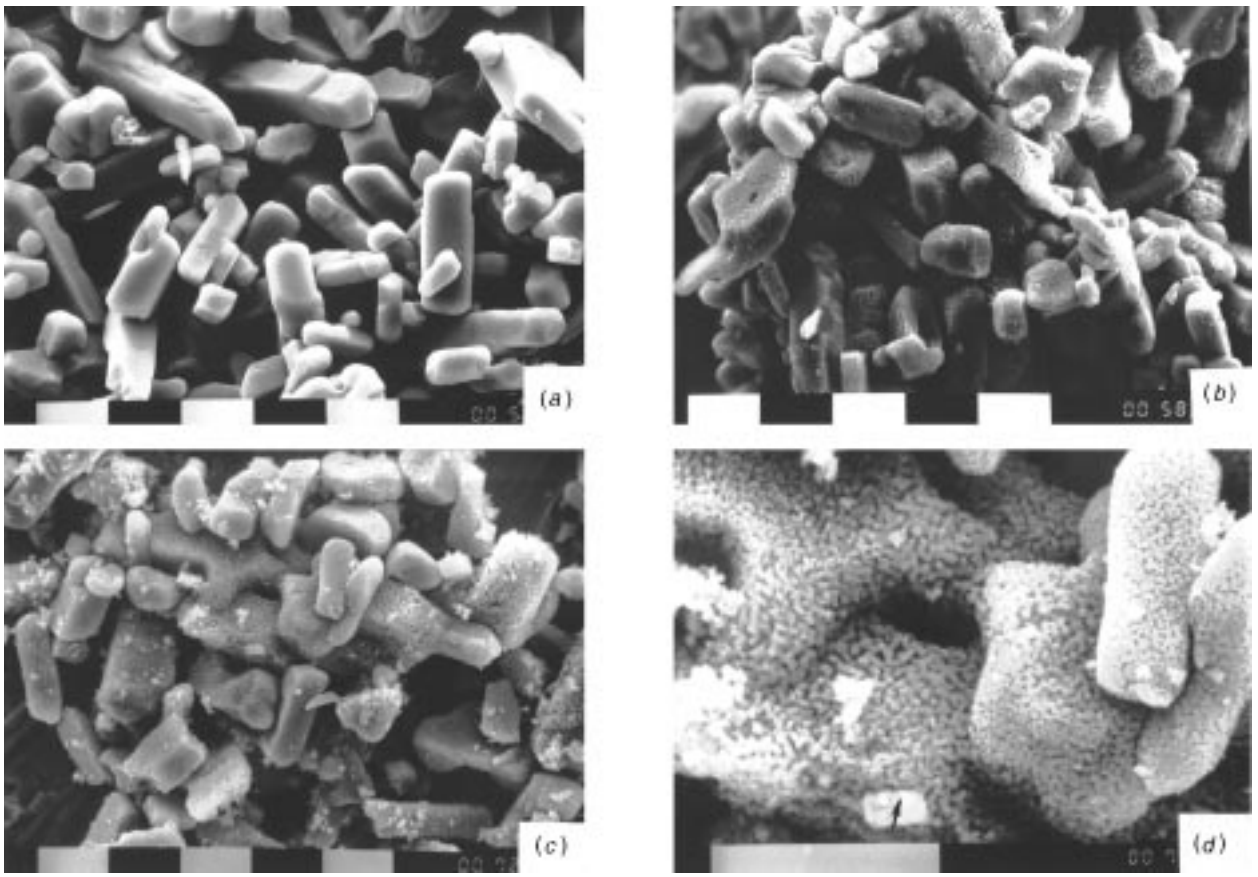

Fig. 5 SEM micrographs of the β-$V_9Mo_6O_{40}$ phase: (*a*) original sample (magnification × 1500, scale bar = 10 mm); (*b*) recovered after the first reduction peak in the TPR at $\beta = 2.5$ K min^{-1} (magnification × 1500, scale bar = 10 mm); (*c*) recovered after the second reduction peak in the TPR at $\beta = 2.5$ K min^{-1} (magnification × 1500, scale bar = 10 mm); (*d*) detail of (*c*) (magnification × 3000, scale bar = 10 mm). The arrow in (*d*) corresponds to the spot analysis giving the highest content of vanadium (see Table 3).

Table 3 Results of the EDS analysis on oxidised and reduced β-$V_9Mo_6O_{40}$ samples (heating rate β/K min^{-1})

			reduced (TPR at 973 K)[b]			reduced (TPR at 1273 K)[c]	
element	theor.[a]	as prepared	$\beta = 5$	$\beta = 2.5$	$\beta = 1$	$\beta = 5$	
%V	44	44	38	39	43	42	66[d]
%Mo	56	56	62	61	57	58	34[d]

[a]The theoretical content of V and Mo has been calculated according to the formula $V_9Mo_6O_{40}$. [b]Samples recovered after the first reduction peak in the TPR runs at different heating rates, β (see text). [c]Sample recovered after the second reduction peak in the TPR run at $\beta = 5$ K min^{-1} (see text). [d]Spot analysis of a specific point, as indicated by the arrow in Fig. 5(*d*).

crystallinity of the reduced samples was also affected and decreased from the diffraction pattern 1B(*a*) to the diffraction pattern 1B(*c*) according to the final temperature of the TPR run decreasing from (*a*) to (*c*).

Temperature-programmed reduction

The TPR profile at $\beta = 5$ K min^{-1} of the β-$V_9Mo_6O_{40}$ phase is characterized by two resolved peaks centred at T_M values of *ca.* 900 and 1130 K. The single peak at lower temperature may represent a simultaneous reduction of Mo^{6+}, V^{5+} and V^{4+} cations forming originally the β-$V_9Mo_6O_{40}$ phase or, alternatively, a sequence of reduction steps that are unresolved under the employed experimental conditions. In order to discriminate between these two hypotheses, TPR runs were carried out at lower heating rates of 2.5 and 1 K min^{-1} to improve the resolution of the reduction profiles. In spite of the decrease of the heating rate at 2.5 K min^{-1} and the consequent increase in resolution, the peak at lower temperature ($T_M = 863$ K) is not split into more components and not even shoulders are evident. On decreasing further the heating rate to 1 K min^{-1}, the lower temperature peak still appears as a single peak centred at $T_M = 833$ K. These results clearly suggest that the reduction of Mo^{6+}, V^{5+} and V^{4+} ions occurs simultaneously in the β-$V_9Mo_6O_{40}$ crystal lattice which decomposes forming in the first step MoO_2 and V_2O_3. The latter conclusion was supported both by quantitative TPR analysis and XRPD carried out on the samples recovered in the TPR runs stopped as the first peak appeared. A further result provided by TPR analysis is that the T_M value of the first reduction peak of the β-$V_9Mo_6O_{40}$ phase is much lower than the T_M values of the TPR peaks found under similar experimental conditions for pure MoO_3 and V_2O_5 and corresponding, respectively, to the reduction to MoO_2 and V_2O_3. This remarkable shift towards lower temperature is a clear evidence that all the cations in the β-$V_9Mo_6O_{40}$ phase are reciprocally affected through a cooperative catalytic effect which enhances their reducibility. Moreover, these results agree well with those obtained by the IR analysis showing that, with respect to the bulk MoO_3 and V_2O_5 oxides, the arrangement of the lattice oxygen in the β-$V_9Mo_6O_{40}$ phase is affected by the simultaneous presence of molybdenum and vanadium cations (*vide infra*). On the other hand, the reducibility of the β-$V_9Mo_6O_{40}$ phase can be compared to that observed in some reduced iso- and hetero-polymetalates (heteropoly blues) in which the electronic structure of the individual polyhedra plays an important role.[21] Some studies of intensely coloured Keggin, Dawson and related phases suggest that the bonding is not extensively delocalised.[21] If this is the case also for the β-$V_9Mo_6O_{40}$ phase, this explains well its enhanced reducibility with respect to the

bulk oxides and the preservation of the original structure upon mild reduction. The IR and EPR results (*vide infra*) indeed support this point of view. Incidently, the Keggin, Dawson and related phases belong to a group of mixed-valence compound where the elements with two oxidation states are located in rather similar sites differing only by small changes in the bond lengths or angles, but which in principle can be distinguished crystallographically.

The second TPR peak appearing at higher temperature corresponds to the reduction of MoO_2 to Mo^0, as confirmed also by the XRPD analysis. No metal vanadium was detected. This is in agreement with the thermodynamics: V_2O_3 is more stable than MoO_2 [$\Delta G^0_f(V_2O_3) = -1137.67$ kJ mol^{-1}; $\Delta G^0_f(MoO_2) = -532.28$ kJ mol^{-1}] and, consequently, is more difficult to reduce to metal with respect to the latter. The results of the quantitative analysis concerning the first (low-temperature) reduction peak showed that the hydrogen consumption was almost equal to the amount of water formed by reduction. Accordingly, both these quantities were indicated in Table 1 as single S_o values. For each heating rate, both the hydrogen consumption and the water formed by reduction were consistent with the following stoichiometry:

$$V_9Mo_6O_{40} + 29/2\ H_2 \rightarrow 9/2\ V_2O_3 + 6\ MoO_2 + 29/2\ H_2O \quad (2)$$

Therefore the TPR quantitative data and the XRPD results are in agreement. However, a significant difference between the experimental and theoretical S_o values was observed for the TPR run at the highest heating rate (see Table 1). Taking into account that the theoretical S_o value has been calculated on the basis of eqn. (2), the higher experimental S_o value (higher hydrogen consumption and an equally higher amount of water formed by reduction) can be attributed to an overlap between the end of the first reduction process, represented by eqn. (2) and the beginning of the second reduction process, described by the following equation:

$$MoO_2 + 2\ H_2 \rightarrow Mo^0 + 2\ H_2O \quad (3)$$

The overlap between the consecutive reduction processes represented by eqn. (2) and (3) tends to increase with an increase in the heating rate. On the contrary, on lowering the heating rate the reaction is slowed and it is easier to separate the end of the first reduction step from the beginning of the second. This explains well the best agreement between the experimental and calculated value of S_o for the TPR run carried out at the lowest heating rate ($\beta = 1$ K min^{-1}, Table 1).

IR spectroscopy

The IR spectra of some members of the $(Mo_xV_{1-x})_2O_5$ ($0.1 < x < 0.3$) solid solution and of the β-$V_9Mo_6O_{40}$ phase have been reported in previous work.[3,12,22,23]

From Fig. 3A it is clearly seen that the V—O and Mo—O bands of the β-$V_9Mo_6O_{40}$ phase do not overlap the MoO_3 and V_2O_5 spectra. This suggests that the arrangement of the lattice oxygen is affected by the simultaneous presence of molybdenum and vanadium cations. The bands in the higher wavenumber region (987, 962–925 cm^{-1}) can be related to the stretching vibrations of the V—O and Mo—O bonding, whereas the very broad band centered at 797 cm^{-1} is associated with the vibrations of the polymeric metal—O—metal chains.[3] An interesting feature is that these bands are shifted to lower frequencies than those observed for similar vibrations in the spectra of both V_2O_5 and MoO_3 as well as $(Mo_xV_{1-x})_2O_5$ solid solutions. This trend is expected on the basis of a decrease of the bond lengths and bond orders of metal–oxygen bonding. If it is the case, such a decrease of the bond lengths and bond orders of metal–oxygen bonding may influence the solid reducibility thus providing a further explanation as to why the β-$V_9Mo_6O_{40}$ phase is reduced more easily than the pure V_2O_5 and MoO_3 oxides, as evidenced by TPR analysis. It is noticeable that the shorter (Mo,V)—O distance (1.659 Å), reported in the first structural study of the $V_9Mo_6O_{40}$ compound, is intermediate between the bond lengths of MoO_3 (1.671 Å) and of V_2O_5 (1.585 Å).[18] Compared to the spectrum 3B(*a*) of the as-prepared β-$V_9Mo_6O_{40}$ phase, the spectra 3B(*b*)–(*d*) of the samples reduced in the TPR runs stopped at 623, 723 and 823 K are characterized by a gradual deformation of the original bands. Moreover a shift towards lower frequencies in the 900 and 550 cm^{-1} region was observed. This may be related to a progressive increase in the number of V^{4+} ions, as indeed found by EPR analysis (*vide infra*), leading to a weakening of the metal–oxygen vibrations. These data, supported by TPR analysis, point out that up to 823 K only a mild reduction of the original β-$V_9Mo_6O_{40}$ phase occurred. Furthermore, the IR analysis of the slightly reduced β-$V_9Mo_6O_{40}$ phase reported in this work seems to be in agreement with a recent IR study of reduced heterododecamolybdates showing that the reduction of the Keggin anion with one electron did not result in dramatic changes of the IR spectra, only revealing a shift and splitting of some bands and the preservation of the original structure.[24]

The spectrum 3B(*g*) of the sample recovered after TPR at 923 K is characterised by additional weak bands located in the 750 cm^{-1} region, which can be assigned to the Mo^{4+}—O vibrations of the MoO_2 lattice. On the other hand, the sample reduced at a temperature high enough (TPR at 1273 K) to attain the complete molybdenum reduction shows a spectrum [3B(*h*)] similar to that of V_2O_3 [3B(*i*)]. This oxide, as the vanadium oxides in the lower oxidation state, has a great tendency to be over-oxidized at the surface by air contact.[25] Therefore the band near 1000 cm^{-1} is associated with the topping (V^{5+}—O) bonds. Spectra 3B(*e*), (*f*), corresponding to samples re-oxidized in air at 773 K for, respectively, 1 and 24 h after TPR at 823 K, resemble that of the as-prepared specimen. It should be recalled that at 823 K the reduction process is just beginning. Therefore the latter spectra suggest that the original structure of a slightly reduced β-$V_9Mo_6O_{40}$ sample can be restored by simply re-heating the solid in air.

EPR spectroscopy

The EPR spectrum at RT of the as-prepared β-$V_9Mo_6O_{40}$ sample consists of an intense and slightly asymmetrical line ($\Delta H_{pp} = 140$ G) with $g_{av} = 1.94$, typical of V^{4+} ions. At 77 K the linewidth becomes sharper and appears a typical axial spectrum characterised by the absence of any hyperfine structure and by $g_{\parallel} = 1.875$ and $g_{\perp} = 1.969$ ($\Delta H_{PP\parallel} = 50$ G and $\Delta H_{pp\perp} = 30$ G). According to the formula $g_{av} = (g_{\parallel} + 2\,g_{\perp})/3$, an average value of 1.938 can be calculated which is in good agreement with that obtained at RT. The absence of a hyperfine structure, observed in systems containing isolated V^{4+} ions, is due to exchange interactions. When these interactions are dominating, a narrowing effect and a Lorentzian line shape of the EPR signal occur.[26] Exchange-narrowed spectra indeed characterised not only the β-$V_9Mo_6O_{40}$ samples but also two standards used in this work, *i.e.* $VOSO_4 \cdot 5H_2O$ and $VO(acac)_2$. In all cases a good fit was obtained between the experimental spectra and those simulated by assuming a Lorentzian lineshape. The sample recovered from the TPR experiment stopped at 823 K gives, at RT, an EPR spectrum similar to that recorded before the treatment: the only difference is that the line is more symmetrical with a slight increase in the linewidth ($\Delta H_{pp} = 150$ G). Also the spectrum recorded at 77 K still consists of a single asymmetrical line with the same g_{av} value (1.94) and a slightly sharper linewidth ($\Delta H_{pp} = 120$ G). On the other hand a marked decrease in intensity characterised the EPR spectrum at RT of the sample recovered after the TPR run stopped at 950 K.

Interestingly, by comparing in the as-prepared β-$V_9Mo_6O_4$

phase the number of spins g^{-1} with the number of V ions g^{-1} (3.24×10^{21}), the percentage of V^{4+} estimated by EPR (*ca.* 9%) is very close to the theoretical value (11%). By taking into account the accuracy of the absolute EPR determinations, from these results it can be inferred that almost all V^{4+} ions in the β-$V_9Mo_6O_{40}$ compound contribute to the EPR signal. The number of spins g^{-1} of the reduced specimen as recovered after the TPR run at 823 K increased by a factor two when compared to the original sample, whereas the main characteristics of the EPR spectrum, *i.e.* the *g* factor, the linewidth and its dependence on the temperature, remained rather similar. A reasonable explanation of these results may be that, upon reduction at 823 K, the fraction of the paramagnetic species increased but their environment was not remarkably affected, as indeed supported by the IR spectra. The signal broadening is likely a consequence of the disorder produced in the crystal lattice by the H_2 treatment which likely induces less efficient exchange interactions. As shown by TPR, at 823 K the reduction process is just commencing and the β-$V_9Mo_6O_{40}$ structure seems to be largely preserved with only an increase of the fraction of the V^{4+} cations. By contrast, a strong decrease of the signal intensity was indeed found for the sample recovered from the TPR run stopped at 950 K suggesting that the V^{4+} ions were almost completely reduced to V^{3+} ions in agreement with the XRD and TPR data.

SEM/EDS

The SEM micrographs show the initial morphology of the β-$V_9Mo_6O_{40}$ phase and its changes occurring at different steps of the reduction process. The original monoclinic β-$V_9Mo_6O_{40}$ phase is characterized by crystals having a rather well defined shape [see Fig. 5(*a*)]. The morphology of the as-prepared sample seems to be not remarkably affected upon reduction. The sample recovered after the first reduction peak in the TPR run at $\beta = 2.5$ K min^{-1} still showed prismatic crystals, mainly belonging to the MoO_2 monoclinic phase, mixed with quasi-spherical V_2O_3 oxide particles [see Fig. 5(*b*)]. However, on the surface of most prismatic crystals appeared a microroughness which may be related to the incipient formation of molybdenum metal. This hypothesis was supported by the micrograph of the sample recovered after the second reduction peak in the TPR run at $\beta = 2.5$ K min^{-1} [Fig. 5(*c*)] where the complete reduction of MoO_2 to metal occurred. Crystals of this sample are indeed characterized by a widespread and more marked microroughness, as is clearly evident by the morphology details shown in Fig. 5(*d*).

The EDS analysis of the samples recovered after the first reduction peak in the TPR runs at $\beta = 2.5$ and 5 K min^{-1} revealed that the Mo and V average contents were rather similar to each other but slightly different from those found for the sample reduced in the TPR run at 1 K min^{-1}. In fact the chemical analysis of this latter specimen is almost equal to that of the as prepared sample (Table 3). This difference may be related to the incipient formation of molybdenum metal which occurred in the TPR runs at $\beta = 2.5$ and 5 K min^{-1}. The crystal morphology of the sample recovered after the TPR run at 1273 K is shown in Fig. 5(*c*) and, in detail, in Fig. 5(*d*). The amounts of V and Mo found on the large, rough particles were rather different from those detected on the smaller, smooth, white aggregates located on the top. The white aggregates are in fact more rich in vanadium [see the arrow in Fig. 5(*d*) indicating the spot analysis], this suggesting that they are enriched in the V_2O_3 phase. Since V_2O_3 and Mo^0 were formed upon reduction at 1273 K, the roughness at the surface of the larger particles may be related to the metal phase. It should be recalled that the reduction behaviour observed for the β-$V_9Mo_6O_{40}$ phase does not entirely resemble that observed in the reduction process of other Mo-containing mixed oxides in which the high-temperature stable oxidic phases were simultaneously segregated with the metal showing comparable sizes.[6,27]

Conclusions

The β-$V_9Mo_6O_{40}$ phase was obtained by heating to 973 K suitable amounts of MoO_3 and V_2O_5 oxides. The TPR and XRPD study has shown that the β-$V_9Mo_6O_{40}$ phase de-aggregates upon reduction in H_2 by forming in a first step MoO_2 and V_2O_3 at *ca.* 900 K, followed by a second reduction step at higher temperature, *ca.* 1130 K, where the reduction of MoO_2 to molybdenum metal takes place. The reduction of V^{5+} ions of the β-$V_9Mo_6O_{24}$ phase to V_2O_3 occurs *ca.* 100 K lower than that observed for V_2O_5. The enhanced reactivity of the V^{5+} ions in the Mo containing compound is likely an effect of the simultaneous presence of V^{4+} and Mo^{6+} ions in the crystal lattice. This hypothesis is supported by the IR analysis which showed that both the metal–oxygen bonding and the arrangement of the lattice oxygen are affected by the presence of V^{4+} and Mo^{6+} ions in the β-$V_9Mo_6O_{40}$ phase. The EPR spectra were typical for V^{4+} ions which, in the as-prepared sample, appear all to contribute to the signal. The EPR signal of the reduced samples increased upon reduction up to 823 K suggesting that the fraction of the paramagnetic species increased at this temperature which, as evidenced by TPR analysis, corresponds to the commencement of the reduction process. On the other hand, the very weak EPR signal found for the sample reduced by TPR at 950 K indicated that the V^{4+} cations were almost completely reduced at this temperature, in agreement with the TPR and XRPD data. The SEM investigation showed that the morphology of the as prepared sample is characterised mainly by prismatic crystals of different sizes. The original morphology is still preserved upon reduction and a microroughness, related to the formation of molybdenum metal, appears at the surface of the prismatic crystals. Finally, as indicated by IR analysis, upon mild reduction the structure of the β-$V_9Mo_6O_{40}$ phase is still preserved and only a distortion of the crystal lattice occurs. Moreover, the structural distortion of the slightly reduced β-$V_9Mo_6O_{40}$ phase can be recovered by re-heating the solid in air.

This work was supported by CONICET (CEQUINOR-CINDECA) (Argentina) and by CNR (Italy). I. L. B. wishes to thank JEPA Foundation (Italy).

References

1 A. Jones and B. McNicol, *Temperature Programmed Reduction for Solid Materials Characterization*, Marcel Dekker Inc., New York, 1986.
2 S. K. Bhattacharyya, Y. Janakiram and N. D. Ganguly, *J. Catal.*, 1967, **8**, 128.
3 J. Svachula, L. J. Alemany, M. A. Larrubia and J. Tichy, *React. Kinet. Catal. Lett.*, 1993, **49**, 145.
4 J. Machek, J. Svachula and J. Tichy, *II Word Congress and IV European Workshop Meeting New Developments in Selective Oxidation*, ed. V. Cortes Corberan and S. VicBellon, 1993, P25–1.
5 R. H. Munch and E. D. Pierron, *J. Catal.*, 1964, **3**, 406.
6 I. L. Botto and M. Vassallo, *Thermochim. Acta*, 1996, **279**, 205.
7 A. Baiker and D. Monti, *J. Catal.*, 1985, **91**, 361.
8 D. Ballivet Tkatchenko and G. Delahay, *J. Therm. Anal.*, 1994, **41**, 1141.
9 L. E. Briand, L. Gambaro and H. Thomas, *J. Therm. Anal.*, 1995, **44**, 803.
10 R. H. Jarman, P. G. Dickens and A. J. Jacobson, *Mater. Res. Bull.*, 1982, **17**, 325.
11 F. Y. Robb, W. S. Glausinger and P. Courtine, *J. Solid State Chem.*, 1979, **30**, 171.
12 V. L. Volkov, G. Sh. Tynkacheva, A. A. Fotiev and E. V. Tkachenko, *Russ. J. Inorg. Chem.*, 1972, **17**, 1469.
13 G. Fierro, M. Lo Jacono, M. Inversi, P. Porta, R. Lavecchia and F. Cioci, *J. Catal.*, 1994, **148**, 709.

14 D. A. M. Monti and A. Baiker, *J. Catal*., 1983, **83**, 323.
15 D. Cordischi, M. C. Campa, V. Indovina and M. Occhiuzzi, *J. Chem. Soc., Faraday Trans*., 1994, **90**, 207.
16 H. Bosh, B. J. Kip, J. G. van Ommen and P. J. Gellings, *J. Chem. Soc., Faraday Trans. 1*, 1984, **80**, 2479.
17 J. R. Regalbuto and Jin-Wook Ha, *Catal. Lett*., 1994, **29**, 189.
18 L. Kihlborg, *Acta Chem. Scand*., 1967, **21**, 2497.
19 R. H. Jarmen and A. K. Cheetham, *Mater. Res. Bull*., 1982, **17**, 1011.
20 B. Hyde and S. Andersson, *Inorganic Crystal Structures*, John Wiley & Sons, New York, 1989.
21 M. T. Pope, in *Heteropoly and Isopoly Oxometalates*, Springer Verlag, Berlin, New York, Tokyo, 1983.
22 H. Schadow, H. Oppermann and B. Wehner, *Z. Anorg. Allg. Chem*., 1995, **621**, 624.
23 T. Hirata and H.-Y. Zhu, *J. Phys.: Condens. Matter*., 1992, **4**, 7377.
24 M. Fournier, C. Rocchiccioli-Deltcheff and L. P. Kazansky, *Chem. Phys. Lett*., 1994, **223**, 297.
25 J. Mendialdua, R. Casanova, Y. Barbaux, *J. Electron Spectrosc. Relat. Phenom*., 1995, **71**, 249.
26 A. Abragam and B. Bleaney, in *Electron Paramagnetic Resonance of Transition Ions*, Clarendon Press, Oxford, 1970.
27 C. I. Cabello, I. L. Botto and H. Thomas, *Thermochim. Acta*, 1994, **232**, 183.

Paper 7/02111I; *Received* 26*th March*, 1997